Estimation and Control of Wind Turbine Tower Vibrations Based on Individual Blade-Pitch Strategies

Lio, Wai Hou; Jones, Bryn Ll; Rossiter, J. Anthony

Published in:
IEEE Transactions on Control Systems Technology

Link to article, DOI:
10.1109/TCST.2018.2833064

Publication date:
2019

Document Version
Peer reviewed version

Estimation and control of wind turbine tower vibrations based on individual blade-pitch strategies

Wai Hou Lio[1], Bryn Ll. Jones[2] and J. Anthony Rossiter[2].

***Abstract*—In this paper, we present a method to estimate the tower fore-aft velocity based upon measurements from blade load sensors. In addition, a tower dampening control strategy is proposed, based upon an individual blade pitch control architecture that employs this estimate. The observer design presented in this paper exploits the Coleman transformations that convert a time-varying turbine model into one that is linear and time-invariant, greatly simplifying the observability analysis and subsequent observer design. The proposed individual pitch-based tower controller is decoupled from the rotor speed regulation loop and hence does not interfere with the nominal turbine power regulation. Closed-loop results, obtained from high fidelity turbine simulations, show close agreement between the tower estimates and the actual tower velocity. Furthermore, the individual-pitch-based tower controller achieves similar performance compared to the collective-pitch-based approach but with negligible impact upon the nominal turbine power output.**

***Index Terms*—State estimation of dynamical systems, Kalman filter, active damping control, wind energy.**

I. Introduction

Large wind turbines experience uneven and intermittent aerodynamic loads from the wind and such loads inevitably contribute to fatigue damage upon the turbine structures. In order to manage the competing demands of power capture and load mitigation, most modern turbines employ a combination of control systems based upon blade pitch actuation. Primary amongst these is the use of collective pitch control (CPC) [1], whereby the pitch angle of each blade is adjusted by an equal amount in order to regulate the rotor speed in above rated conditions. In addition, individual pitch control (IPC) and tower damping control can be used to specifically attenuate unsteady loads that play no part in power generation. The IPC provides additional pitch demand signals to each blade in order to balance the loads across the rotor plane, typically in response to measurements of the flap-wise blade root bending moments [2]–[4], whilst tower damping control provides a further adjustment to the collective blade pitch angle in order to reduce excessive tower vibrations, in response to tower fore-aft velocity measurements [5]–[8]. Typically, and for reasons of simplicity of implementation favoured by the industry, IPCs and tower damping controllers are designed separately from the CPC, and carefully in order to avoid cross-excitation [9]–[12].

[1]Wai Hou Lio is with Department of Wind Energy, Technical University of Denmark, DK-4000 Roskilde, Denmark. (e-mail: wali@dtu.dk)

[2]Bryn Ll. Jones and J. Anthony Rossiter are with Department of Automatic Control and Systems Engineering, University of Sheffield, Sheffield, S1 3JD, U.K (e-mail: b.l.jones@sheffield.ac.uk; j.a.rossiter@sheffield.ac.uk)

At present, most tower damping control strategies assume a direct measurement of tower motion, typically from a nacelle-mounted accelerometer (e.g. [4], [13]). However, the turbine blades and tower are dynamically coupled and from an estimator design perspective, such interactions may provide an opportunity for the tower motion to be estimated based upon the blade load measurements that are already available to the IPC. If so, this indicates redundancy in the information provided by the tower motion sensor that can either be exploited in terms of a reduction in sensor count, or for fault tolerant control purposes [14]–[16]. Moreover, typical tower damping control strategies provide an additional blade pitch signal collectively to all the blades in response to the tower velocity [13], that is inevitably coupled with the rotor speed regulation loop, thus, affecting the power output of the turbine. On the other hand, well-designed IPCs are largely decoupled from the CPC, thus there are potential benefits to designing an IPC-based tower damping controller.

The contributions of this paper are thus twofold. Firstly, a tower vibration observer design is proposed that estimates the tower fore-aft velocity based solely upon standard blade-load measurements. Secondly, an individual pitch-based tower damping control strategy is presented that provides the blade pitch command to each blade independently and with little impact on the nominal turbine power regulation.

The remainder of this paper is as follows. Section II presents the model of the blade and tower dynamics. In Section III, a linear, time-invariant (LTI) model is derived that captures the dynamics of the Coleman transform and establishes the coupling between the blade load sensors and tower motion that is key in establishing an observable system. The design of a subsequent tower-top motion estimator and individual pitch-based tower damping controller is described in Section IV. In Section V, the performance of the proposed estimator and controller are demonstrated in simulation upon a high-fidelity and nonlinear wind turbine model.

Notation

Let $\mathbb{R}$, $\mathbb{C}$ and $\mathbb{Z}$ denote the real and complex fields and set of integers, respectively, $j := \sqrt{-1}$ and let $s \in \mathbb{C}$ denote a complex variable. The space $\mathcal{R}$ denotes the space of proper real-rational transfer function matrices and $\dot{x}$ represents the time derivative of x. Let $v^T \in \mathbb{R}^{1\times n_v}$ denote the transpose of a vector $v \in \mathbb{R}^{n_v}$ and $V^T \in \mathbb{R}^{n_y \times n_z}$ is the transpose of a matrix $V \in \mathbb{R}^{n_z \times n_y}$. The identity matrix is denoted as I. Let $\tilde{x}$ denote the deviation of x from its equilibrium x^*.

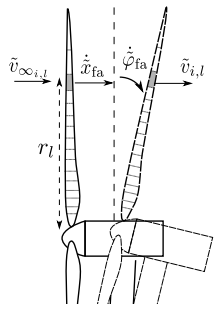

Fig. 1: The perturbation on the free-stream stream-wise wind speed $\tilde{v}_{\infty_{i,l}}$ on the shaded blade element at r_l becomes the apparent wind speed $\tilde{v}_{i,l}$ after the effects of the tower fore-aft velocity $\dot{\tilde{x}}_{\rm fa}$ and rotational velocity $\dot{\tilde{\varphi}}_{\rm fa}$.

II. Modelling

Typically, the dynamics of the blade flap-wise root-bending moment and the tower-top fore-aft motion can be modelled as second-order systems (e.g. [9], [3]), as follows:

$$\ddot{\tilde{M}}_i(t) + 2\zeta_{\rm b}\omega_{\rm b}\dot{\tilde{M}}_i(t) + \omega_{\rm b}^2\tilde{M}_i(t) = \omega_{\rm b}^2\tilde{f}_M(\tilde{\theta}_i, \tilde{v}_i), \tag{1a}$$

$$\ddot{\tilde{x}}_{\rm fa}(t) + 2\zeta_{\rm t}\omega_{\rm t}\dot{\tilde{x}}_{\rm fa}(t) + \omega_{\rm t}^2\tilde{x}_{\rm fa}(t) = \omega_{\rm t}^2\tilde{f}_x(\tilde{\theta}_{\rm col}, \tilde{v}_{\rm col}), \tag{1b}$$

where $\tilde{M}_i(t), \tilde{x}_{\rm fa}(t)$ denote the deviations of the flap-wise blade root bending moment of blade $i \in \{1,2,3\}$ and tower fore-aft displacement from an operating point, respectively. The damping ratio of the blade and tower are $\zeta_{\rm b}, \zeta_{\rm t} \in \mathbb{R}$ and $\omega_{\rm b}, \omega_{\rm t} \in \mathbb{R}$ are the respective natural frequencies of the blade and tower. The nonlinear aerodynamic forcing functions on the blade and tower are typically linearised around the operating wind conditions to obtain the perturbation forces, $\tilde{f}_M(\tilde{\theta}_i, \tilde{v}_i) : \mathbb{R}\times\mathbb{R} \to \mathbb{R}$ and $\tilde{f}_x(\tilde{\theta}_{\rm col}, \tilde{v}_{\rm col}) : \mathbb{R}\times\mathbb{R} \to \mathbb{R}$, defined as follows:

$$\tilde{f}_M(\tilde{\theta}_i, \tilde{v}_i) = \left.\frac{df_M}{d\theta}\right|_{\theta^*,v^*}\tilde{\theta}_i(t) + \left.\frac{df_M}{dv}\right|_{\theta^*,v^*}\tilde{v}_{i,}(t), \tag{1c}$$

$$\tilde{f}_x(\tilde{\theta}_{\rm col}, \tilde{v}_{\rm col}) = \left.\frac{df_x}{d\theta}\right|_{\theta^*,v^*}\tilde{\theta}_{\rm col}(t) + \left.\frac{df_x}{dv}\right|_{\theta^*,v^*}\tilde{v}_{\rm col}(t), \tag{1d}$$

where $\frac{df_M}{d\theta}, \frac{df_x}{d\theta} \in \mathbb{R}$ and $\frac{df_M}{dv}, \frac{df_x}{dv} \in \mathbb{R}$ are the variations of the forcing with respect to the pitch angle and apparent wind speed. The deviations of the blade pitch angle and apparent wind speed from their steady-states $\theta^*, v^* \in \mathbb{R}$ are $\tilde{\theta}_i(t), \tilde{v}_i(t)$, whilst $\tilde{\theta}_{\rm col}(t) := \sum_i \tilde{\theta}_i(t), \tilde{v}_{\rm col}(t) = \sum_i \tilde{v}_i(t)$ denote the perturbations in collective pitch angle and the sum of the wind speed effect on the rotor.

The wind turbine aerodynamic interactions of relevance to this study are depicted in Figure 1. Owing to variable blade geometry, the wind-induced forces are not uniformly distributed on the blades and to model such forces, blade element/momentum theory is adopted [13], where the blade is discretised into small elements. Referring to Figure 1, assuming the blade is rigid, the apparent stream-wise wind speed perturbation $\tilde{v}_{i,l}(t)$ experienced by blade i on span-wise element $l \in \{1,\dots,L\} \subset \mathbb{Z}$ is dependent upon the free-stream wind speed perturbation $\tilde{v}_{\infty_{i,l}}(t)$, deviations of the fore-aft tower-top velocity $\dot{\tilde{x}}_{\rm fa}(t)$ and the tower-top rotational velocity $\dot{\tilde{\varphi}}_{\rm fa}(t)$ from their equilibria, as follows:

$$\tilde{v}_{i,l}(t) = \tilde{v}_{\infty_{i,l}}(t) - \dot{\tilde{x}}_{\rm fa}(t) + \dot{\tilde{\varphi}}_{\rm fa}(t) r_l \sin\big(\phi_i(t)\big), \tag{2a}$$

where $r_l \in \mathbb{R}$ is the radial distance of the l-th blade element. The azimuthal angle of each blade is defined as $[\phi_1(t), \phi_2(t), \phi_3(t)] := [\phi(t), \phi(t) + \frac{2\pi}{3}, \phi(t) + \frac{4\pi}{3}]$, where $\phi(t)$ is the angle of the first blade from the horizontal yaw axis with respect to the clockwise direction. This work implicitly assumes the tower is a prismatic beam so that the ratio between rotation and displacement is $\frac{2}{3h}$, where $h \in \mathbb{R}$ is the height of the tower [3]. Thus, the fore-aft rotational velocity of the tower-top can be approximated as $\dot{\tilde{\varphi}}_{\rm fa}(t) \approx \frac{2}{3h}\dot{\tilde{x}}_{\rm fa}(t)$. Since the focus of this work is on the blade disturbance induced by the wind, the effect of the wind perturbations upon the blade, $\tilde{v}_i(t)$ in (1), can be approximated by averaging the apparent wind speed perturbations $\tilde{v}_{i,l}(t)$ along the blade, as follows:

$$\begin{aligned}\tilde{v}_i(t) &\approx \frac{1}{L}\sum_l \tilde{v}_{i,l}(t),\\ &= \tilde{v}_{\infty,i}(t) - \dot{\tilde{x}}_{\rm fa}(t) + k_\varphi \dot{\tilde{x}}_{\rm fa}(t)\sin\big(\phi_i(t)\big).\end{aligned} \tag{2b}$$

Inspection of (1) and (2) indicates that coupling exists between the dynamics of the blade flap-wise root-bending moment and the tower, which is the key property that underpins the subsequent work in this paper. By substituting (2) into (1), the state-space representation of (1) can be formulated as follows:

$$\begin{aligned}\dot{x}(t) &= A(t)x(t) + Bu(t) + B_{\rm d}d(t),\\ y(t) &= Cx(t),\end{aligned} \tag{3}$$

where $u(t) := [\tilde{\theta}_1(t), \tilde{\theta}_2(t), \tilde{\theta}_3(t)]^T \in \mathbb{R}^{n_u}$ and $y(t) := [\tilde{M}_1(t), \tilde{M}_2(t), \tilde{M}_3(t)]^T \in \mathbb{R}^{n_y}$ are the control inputs and measured outputs, respectively, whilst $d(t) := [\tilde{v}_{\infty,1}(t), \tilde{v}_{\infty,2}(t), \tilde{v}_{\infty,3}(t)]^T \in \mathbb{R}^{n_d}$ are the wind disturbance inputs. The state vector is $x(t) := [\dot{\tilde{M}}_1(t), \dot{\tilde{M}}_2(t), \dot{\tilde{M}}_3(t), \tilde{M}_1(t), \tilde{M}_2(t), \tilde{M}_3(t), \dot{\tilde{x}}_{\rm fa}(t), \tilde{x}_{\rm fa}(t)]^T \in \mathbb{R}^{n_x}$. Notice that the system matrix $A \in \mathbb{R}^{n_x\times n_x}$ is time-dependent owing to the time-varying nature of the azimuth angle.

III. Transformation to an LTI system and observability analysis

For a linear time-varying (LTV) system (3), there exist techniques for observability analysis and estimator design (e.g. [17]). However, the problem of establishing the observability proof and synthesising an estimator for the LTV system (3) can be greatly simplified by reformulating (3) as an LTI system. As will now be shown, the key to achieving this lies in the use of a coordinate transformation based upon the Coleman Transform.

The Coleman Transform projects the blade loads in the rotating frame of reference onto the fixed tilt and yaw turbine axes. The typical Coleman transform $T_{\rm cm}\big(\phi(t)\big) \in \mathbb{R}^{3\times 3}$ is

defined as follows (e.g. [10] and references therein):

$$[\tilde{M}_{\mathrm{col}}(t), \tilde{M}_{\mathrm{tilt}}(t), \tilde{M}_{\mathrm{yaw}}(t)]^T = T_{\mathrm{cm}}\big(\phi(t)\big)[\tilde{M}_1(t), \tilde{M}_2(t), \tilde{M}_3(t)]^T, \tag{4a}$$

$$T_{\mathrm{cm}}\big(\phi(t)\big) := \frac{2}{3}\begin{bmatrix} \frac{1}{2} & \frac{1}{2} & \frac{1}{2} \\ \sin\big(\phi(t)\big) & \sin\big(\phi(t)+\frac{2\pi}{3}\big) & \sin\big(\phi(t)+\frac{4\pi}{3}\big) \\ \cos\big(\phi(t)\big) & \cos\big(\phi(t)+\frac{2\pi}{3}\big) & \cos\big(\phi(t)+\frac{4\pi}{3}\big) \end{bmatrix}, \tag{4b}$$

where $\tilde{M}_{\mathrm{col}}(t), \tilde{M}_{\mathrm{tilt}}(t), \tilde{M}_{\mathrm{yaw}}(t)$ denote the perturbation on the collective, tilt and yaw referred flap-wise blade root-bending moments, respectively. The inverse Coleman transform $T_{\mathrm{cm}}^{\mathrm{inv}}\big(\phi(t)\big) \in \mathbb{R}^{3\times 3}$ is as follows:

$$[\tilde{\theta}_1(t), \tilde{\theta}_2(t), \tilde{\theta}_3(t)]^T = T_{\mathrm{cm}}^{\mathrm{inv}}\big(\phi(t)\big)[\tilde{\theta}_{\mathrm{col}}(t), \tilde{\theta}_{\mathrm{tilt}}(t), \tilde{\theta}_{\mathrm{yaw}}(t)]^T, \tag{4c}$$

$$T_{\mathrm{cm}}^{\mathrm{inv}}\big(\phi(t)\big) := \begin{bmatrix} 1 & \sin\big(\phi(t)\big) & \cos\big(\phi(t)\big) \\ 1 & \sin\big(\phi(t)+\frac{2\pi}{3}\big) & \cos\big(\phi(t)+\frac{2\pi}{3}\big) \\ 1 & \sin\big(\phi(t)+\frac{4\pi}{3}\big) & \cos\big(\phi(t)+\frac{4\pi}{3}\big) \end{bmatrix}, \tag{4d}$$

where $\tilde{\theta}_{\mathrm{col}}(t), \tilde{\theta}_{\mathrm{tilt}}(t), \tilde{\theta}_{\mathrm{yaw}}(t)$ represent the perturbations on the collective pitch and the referred pitch signals upon the tilt and yaw axis, respectively. The same also applies to the wind speed $\tilde{v}_i$.

Clearly, the Coleman Transforms are time-dependent, and hence their dynamics must be factored into any system model that employs them. As shown in [10] from the perspective of IPC design, models that arise from the misconceived treatment of the Coleman Transforms as static projections give rise to erroneous dynamics, leading to poor IPC performance. Thus, this work presents the LTI reformulation of (3) with the correct treatment of the Coleman Transforms in Theorem 3.1.

Theorem 3.1: Assuming a fixed rotor speed and Coleman transformations (4), the linear time-varying system (3) can be transformed into the following LTI form:

$$\begin{aligned} \dot{\xi}(t) &= A_\xi \xi(t) + B_\xi u_{\mathrm{cm}}(t) + B_{\xi\mathrm{d}} d_{\mathrm{cm}}(t), \\ y_{\mathrm{cm}}(t) &= C_\xi \xi(t), \end{aligned} \tag{5}$$

where $y_{\mathrm{cm}}(t) = [\tilde{M}_{\mathrm{col}}(t), \tilde{M}_{\mathrm{tilt}}(t), \tilde{M}_{\mathrm{yaw}}(t)]^T \in \mathbb{R}^{n_y}$, $u_{\mathrm{cm}}(t) = [\tilde{\theta}_{\mathrm{col}}(t), \tilde{\theta}_{\mathrm{tilt}}(t), \tilde{\theta}_{\mathrm{yaw}}(t)]^T \in \mathbb{R}^{n_u}$, $d_{\mathrm{cm}}(t) = [\tilde{v}_{\infty,\mathrm{col}}(t), \tilde{v}_{\infty,\mathrm{tilt}}(t), \tilde{v}_{\infty,\mathrm{yaw}}(t)]^T \in \mathbb{R}^{n_d}$ are the referred measurements of the flap-wise blade moments, pitch angle signals and wind speeds upon the fixed reference frame, whilst $\xi(t) \in \mathbb{R}^{n_\xi}$ is the projection of the states associated with the blade dynamics upon a non-rotating reference frame (19) and the states of the tower dynamics (20).

Proof: See Appendix A. ∎

Corollary 1: Assuming the model parameters obtained from linearising the baseline turbine [18], the system (5) is observable.

Proof: Trivial inspection of the rank of the system's observability matrix. ∎

Hence, the tower motion states are observable from measurements of the blade loads alone. This result lays the foundation for the observer and controller designs of the next section.

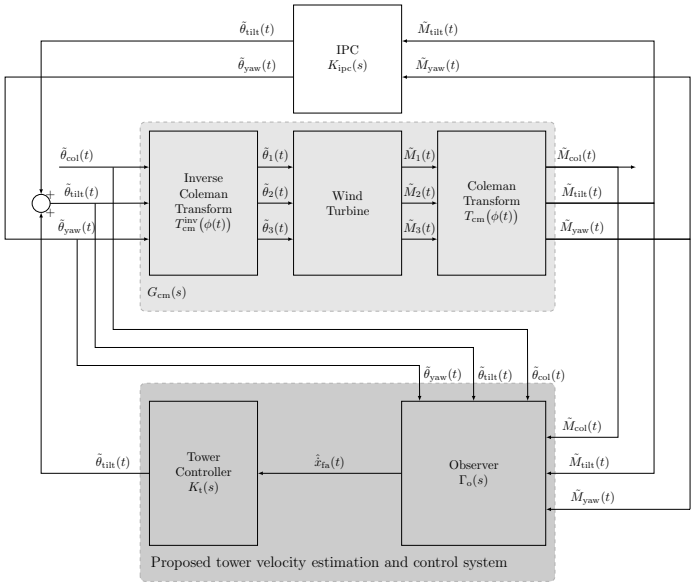

Fig. 2: Schematic of the proposed estimator and controller.

IV. Design of the Estimator and Controller

Figure 2 depicts the architecture of the proposed estimation and control system, where the tower motion estimator produces an estimate $\hat{\dot{x}}_{\mathrm{fa}}(t)$ of the fore-aft velocity of the tower-top based on Coleman-transformed blade moment measurements $\tilde{M}_{\mathrm{col}}(t), \tilde{M}_{\mathrm{tilt}}(t), \tilde{M}_{\mathrm{yaw}}(t)$ and pitch signals $\tilde{\theta}_{\mathrm{col}}(t), \tilde{\theta}_{\mathrm{tilt}}(t), \tilde{\theta}_{\mathrm{yaw}}(t)$. The individual pitch-based tower controller subsequently employs this estimate to provide additional referred blade pitch signals upon the tilt axis $\tilde{\theta}_{\mathrm{tilt}}(t)$ for attenuating the tower motion. Note that this architecture is deliberately chosen so as to augment, rather than replace the existing turbine controllers.

A. Estimator design

The system (5) is driven by the wind-induced disturbance, which consists of slow-moving mean wind speeds and fast-changing turbulence. We consider these wind speed disturbances as coloured noise. Given the known frequency spectra of these wind speed disturbances, a linear wind model that is driven by Gaussian white noise $w(t) \in \mathbb{R}^{n_d}$ is defined as follows:

$$\dot{\xi}_w(t) = A_w \xi_w(t) + B_w w(t),\ d_{\mathrm{cm}}(t) = C_w \xi_w(t), \tag{6}$$

where the system matrices $\{A_w, B_w, C_w\}$ are determined by fitting the spectra of the model output to the known spectra of the wind speed disturbances. Combining the LTI system (5) and the wind disturbance model (6), we yield the proposed tower observer as follows:

$$\begin{aligned} \dot{x}_{\mathrm{a}}(t) &= A_{\mathrm{a}} x_{\mathrm{a}}(t) + B_{\mathrm{a}} u_{\mathrm{cm}}(t) + L e(t), \\ y_{\mathrm{cm}}(t) &= C_{\mathrm{a}} x_{\mathrm{a}}(t), \end{aligned} \tag{7}$$

where $x_{\mathrm{a}}(t) = [\xi(t), \xi_w(t)]^T \in \mathbb{R}^{n_{x_{\mathrm{a}}}}$ denotes the state of the augmented system, whilst $L \in \mathbb{R}^{n_{x_{\mathrm{a}}} \times n_y}$ is a steady-state Kalman filter gain and $e(t) \in \mathbb{R}^{n_y}$ is the prediction error between the plant and model output.

B. Estimation-based controller design

Typically, a tower controller provides an additional collective blade pitch signal on top of the CPC loop in response to the tower fore-aft velocity, in order to dampen the fore-aft structural mode. The excessive vibrations of the tower are mainly concentrated around the resonant frequency of the tower (0.32Hz in this work) [13]. However, the collective-pitch-based approach might affect the rotor speed regulation loop performance. Thus, this work proposes a novel tower damping strategy using the existing Coleman transform-based IPC architecture to decouple the CPC and IPC loops. The proposed tower controller uses the referred pitch signal upon the tilt axis in response to the tower-top velocity estimate, as shown in Figure 2. The key challenge is to separate the existing IPC loop and the tower damping control loop, which is particularly important since the tower estimate is also dependent upon the blade load measurements. To see this, firstly consider the LTI system (5) in its transfer function form:

$$y_{\rm cm}(s) = G_{\rm cm}(s)u_{\rm cm}(s). \tag{8}$$

Secondly, consider the existing Coleman transform-based IPC controller $K_{\rm ipc} \in \mathcal{R}^{2\times 2}$, adopted from [11], [19]:

$$\begin{bmatrix}\tilde{\theta}_{\rm tilt}(s)\\ \tilde{\theta}_{\rm yaw}(s)\end{bmatrix} = \begin{bmatrix}K_{\rm ipc}^{(1,1)}(s) & K_{\rm ipc}^{(1,2)}(s)\\ K_{\rm ipc}^{(2,1)}(s) & K_{\rm ipc}^{(2,2)}(s)\end{bmatrix}\begin{bmatrix}\tilde{M}_{\rm tilt}(s)\\ \tilde{M}_{\rm yaw}(s)\end{bmatrix}. \tag{9}$$

Referring to Figure 2, together with the proposed tower controller $K_{\rm t} \in \mathcal{R}$ and the observer $\Gamma_{\rm ob} \in \mathcal{R}^{1\times(n_u+n_y)}$, the pitch signal $\theta_{\rm tilt}$ on the tilt axis becomes:

$$\tilde{\theta}_{\rm tilt}(s) = K_{\rm ipc}^{(1,1)}(s)\tilde{M}_{\rm tilt}(s) + K_{\rm ipc}^{(1,2)}(s)\tilde{M}_{\rm yaw}(s) + K_{\rm t}(s)\hat{X}_{\rm fa}(s), \tag{10}$$

where the estimate of the tower-top fore-aft velocity $\hat{X}_{\rm fa} \in \mathcal{R}$ can be expressed as follows:

$$\hat{X}_{\rm fa}(s) = \Gamma_{\rm ob}(s)[u_{\rm cm}(s), y_{\rm cm}(s)]^T, \tag{11a}$$

$$\Gamma_{\rm ob}(s) := [\Gamma_{\rm ob}^{(1,1)}(s), \Gamma_{\rm ob}^{(1,2)}(s), \Gamma_{\rm ob}^{(1,3)}(s), \ldots \quad \ldots \quad \Gamma_{\rm ob}^{(1,4)}(s), \Gamma_{\rm ob}^{(1,5)}(s), \Gamma_{\rm ob}^{(1,6)}(s)]. \tag{11b}$$

By substituting (11) into (10), the existing IPC $K_{\rm ipc}$ in (9) is inevitably coupled with the tower controller $K_{\rm t}$ and becomes $K_{\rm ipc}^{\rm m} \in \mathcal{R}^{2\times 2}$, where:

$$K_{\rm ipc}^{\rm m}(s) = \begin{bmatrix}K_{\rm ipc}^{{\rm m}(1,1)}(s) & K_{\rm ipc}^{{\rm m}(1,2)}(s)\\ K_{\rm ipc}^{(2,1)}(s) & K_{\rm ipc}^{(2,2)}(s)\end{bmatrix}, \tag{12a}$$

$$K_{\rm ipc}^{{\rm m}(1,1)}(s) = \big(I + K_{\rm t}(s)\Gamma_{\rm ob}^{(1,2)}(s)\big)K_{\rm ipc}^{(1,1)}(s) + \Gamma_{\rm ob}^{(1,5)}(s), \tag{12b}$$

$$K_{\rm ipc}^{{\rm m}(1,2)}(s) = \big(I + K_{\rm t}(s)\Gamma_{\rm ob}^{(1,3)}(s)\big)K_{\rm ipc}^{(1,2)}(s) + \Gamma_{\rm ob}^{(1,6)}(s), \tag{12c}$$

Thus the observer introduces undesirable, but inevitable coupling from the tower controller to the existing IPC. Nonetheless, the Coleman transform-based IPC typically targets the static and 3p (thrice per revolution) non-rotating loads caused by the blade (e.g. 0 and 0.6 Hz) [20], whilst tower loads occur mainly at the tower resonant frequency (0.32Hz). Therefore, with a view towards avoiding the undesired couplings, the tower controller is designed as an inverse notch filter with gain concentrated at the tower resonant frequency, away from multiples of the blade rotational frequency:

$$K_{\rm t}(s) := K_{\rm p}\left(\frac{s^2 + 2D_1\omega_{\rm t}s + \omega_{\rm t}^2}{s^2 + 2D_2\omega_{\rm t}s + \omega_{\rm t}^2}\right), \tag{13}$$

where $K_{\rm p} = 0.03$, $D_1 = 10$ and $D_2 = 0.05$.

To examine the coupling between the existing IPC and the proposed tower controller, Figure 3 shows the closed-loop sensitivity functions of the original IPC controller $S(s) := (I + G_{\rm cm}K_{\rm ipc}(s))^{-1}$ and the coupled controller structure $S^{\rm m}(s) := (I + G_{\rm cm}K_{\rm ipc}^{\rm m}(s))^{-1}$. It is clear from the figure that the disturbance gain of the coupled control structure remains similar to the original IPC, which is also still largely unaffected across all frequencies. In addition, the coupled control structure and the existing controller possesses the same robust stability margin (0.39), suggesting the proposed design does not affect the robustness of the original IPC.

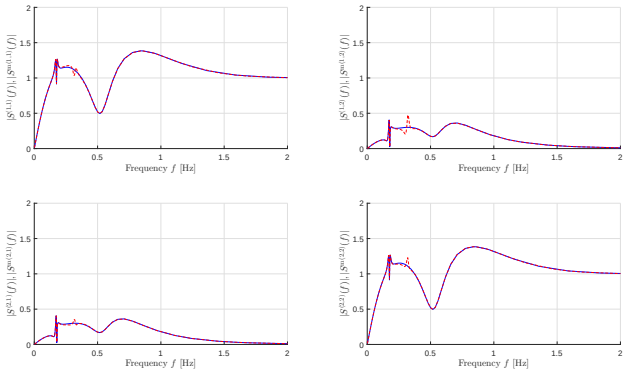

Fig. 3: Magnitude Bode plots of the closed-loop sensitivity functions of $(I + G_{\rm cm}K_{\rm ipc}(s))^{-1}$ (Solid blue line) and $(I + G_{\rm cm}K_{\rm ipc}^{\rm m}(s))^{-1}$ (Dashed red line).

V. Numerical Results and Discussion

This section presents simulation results to demonstrate the performance of the proposed estimator and estimation-based controller for the tower fore-aft motion. The turbine model employed in this work is the NREL 5MW turbine [18] and the simulations are conducted on FAST [21]. This turbine model is of much greater complexity than the linear model (7). All degrees-of-freedom were enabled, including flap-wise and edge-wise blade modes, in addition to the tower and shaft dynamics.

A. Estimator Performance

The proposed observer (7) was compared with a typical double-integrator Kalman-filter design based on measurements from the tower fore-aft accelerometers (e.g. [13]), subsequently referred to as the baseline design. All measurements were perturbed with additive white noise and simulations were conducted under three time-varying wind field test cases: (i) above-rated; (ii) below-rated and (iii) full operating wind conditions.

Simulations in Figure 4 were conducted under a time-varying wind field with a mean wind speed of 18 $\rm ms^{-1}$ and a turbulence intensity of 5%, with the hub-height wind speed shown in Figure 4a. It can be seen that in Figure 4b good agreement was achieved between the proposed and baseline design and actual tower velocity. Nonetheless, small discrepancies for both methods are revealed by evaluating the estimate error magnitude, auto-correlations and spectra, shown in Figures 4c, 4d and 4e, respectively. A residual test [22] was adopted, that suggests the estimate errors would be white noise

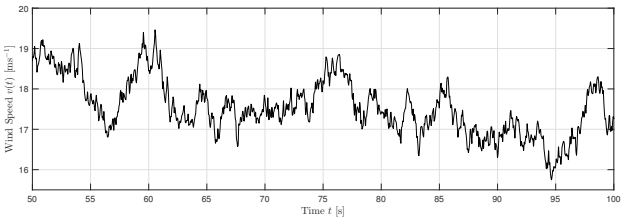

(a) Hub-height wind speed.

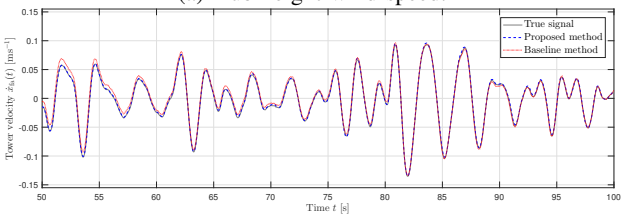

(b) Tower fore-aft velocity.

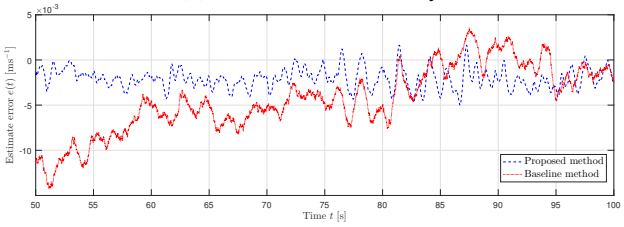

(c) Estimate errors.

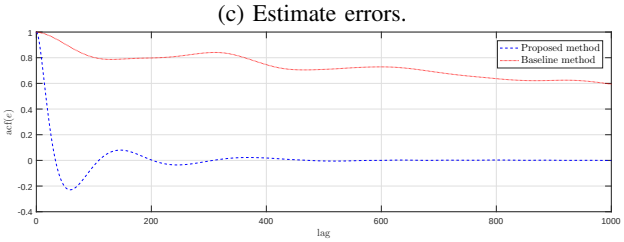

(d) Auto-correlations of the errors.

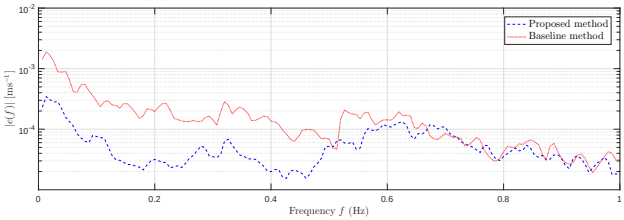

(e) Spectra of the estimate errors.

Fig. 4: Test case (i) with the above-rated wind conditions.

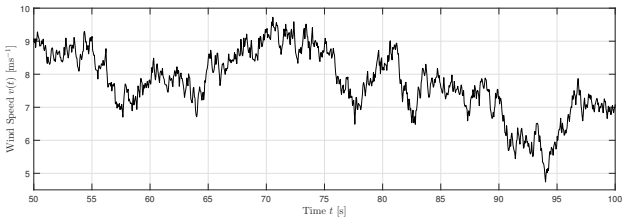

(a) Hub-height wind speed.

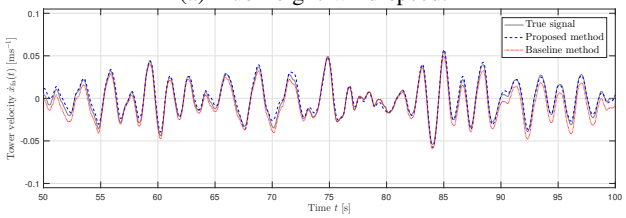

(b) Tower fore-aft velocity.

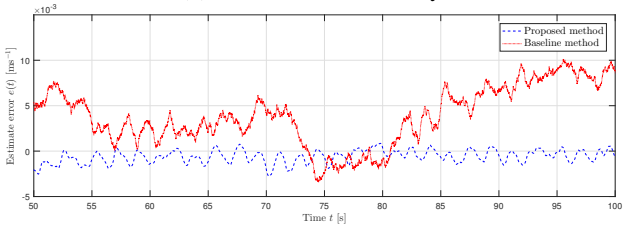

(c) Estimate errors.

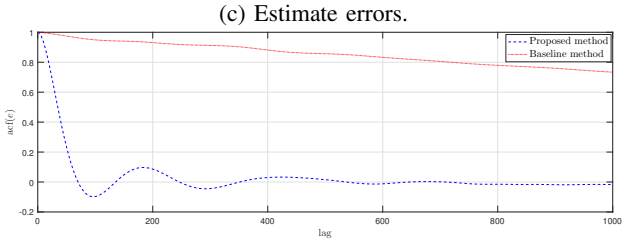

(d) Auto-correlations of the errors.

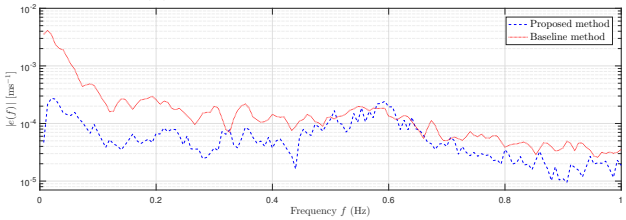

(e) Spectra of the estimate errors.

Fig. 5: Test case (ii) with the below-rated wind conditions.

if perfect models were used by the observer. Figure 4d shows the error correlations, with those of the proposed method being significantly less than the baseline. The improvements in estimation error are obtained in the low frequency range, as shown in Figure 4e.

Similar simulations were conducted for the below-rated wind condition in Figure 5, with mean wind speed of 8 ms^{-1} and turbulence intensity of 5% as shown in Figure 5a. Note that in this test case, the model parameters were linearised around 8 ms^{-1}. The performance and residual tests are shown in Figures 5b, 5c, 5d, and 5e. Figure 5b shows that the proposed and baseline methods both achieved good state estimation. However, compared to the test case (i), the residual test reveals that the estimate errors tend to be larger in the below-rated wind conditions, as shown in Figure 5c and 5e. This is caused by modelling uncertainties since the rotor speed varies significantly in low wind speed conditions. Nonetheless, in Figure 5d, the error auto-correlation for the proposed design is relatively lower than the baseline.

A test case with full operating wind conditions was included, as shown in Figure 6, in order to evaluate the performance of both designs during changing operating conditions. A wind field was increased incrementally by $2\mathrm{ms}^{-1}$ every 20 seconds, as shown in Figure 6a. The proposed design used both observers in the test case (i) and (ii) for the below-rated and above-rated wind conditions. The following heuristic switching policy was employed to overcome the transition between wind conditions:

$$\dot{x}_{\rm fa}(t) = \sum_{\kappa} \rho_{\kappa}(t) \dot{x}_{{\rm fa},\kappa}(t), \quad \sum_{\kappa} \rho_{\kappa}(t) = 1, \tag{14}$$

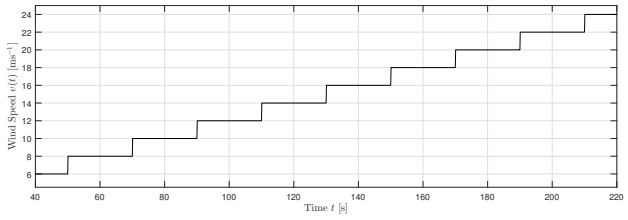

(a) Hub-height wind speed.

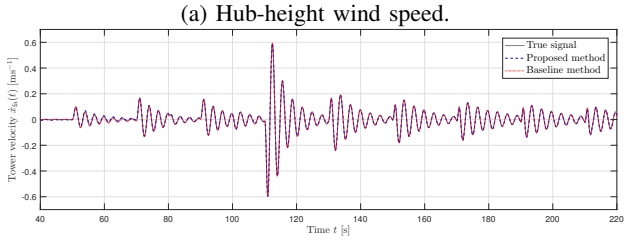

(b) Tower fore-aft velocity.

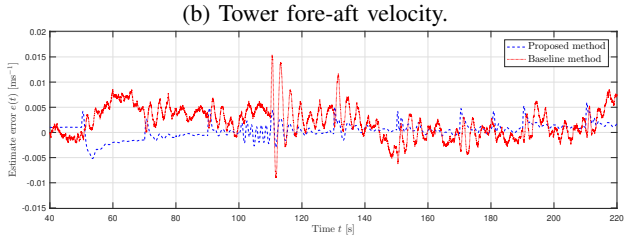

(c) Estimate errors.

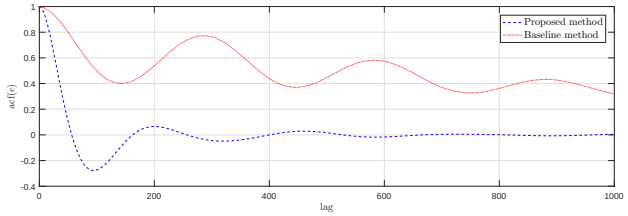

(d) Auto-correlations of the errors.

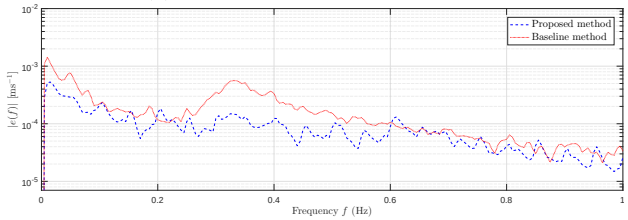

(e) Spectra of the estimate errors.

Fig. 6: Test case (iii) with wind steps in 2ms^{-1} increments across the full operating wind conditions.

where $\kappa \in \{1, 2\}$ is the index of observers designed in the below-rated and above-rated wind conditions, whilst $\rho_\kappa \in \mathbb{R}$ denotes the weighting on the tower estimate of the κ-th estimator. Note that there is no switching policy for the baseline double-integrator model. The performance and residual test of both designs are demonstrated in Figures 6b, 6c, 6d, and 6e. In Figure 6b, good agreement is shown between the true tower signal and the estimates from both the proposed and baseline observers. During the transition of the operating conditions, the switching of turbine controllers caused an oscillation on the tower fore-aft velocity at 110 s, resulting in relatively large errors for both designs. As shown in Figure 6c, the error magnitude from the proposed observer is relatively smaller than that from the baseline. This is because the blade load sensors employed by the proposed method are better able to discern changes in wind and tower loadings on the turbine structure compared to a tower accelerometer. Thus, faster convergence with lower error is achieved, particularly in the low frequency range, as shown in Figure 6e. In addition, in Figure 6d, it is clearly seen that the error auto-correlation of the proposed method was closer to zero, suggesting its residual was almost white noise. That indicates the proposed design together with the switching policy (14) is a more accurate model compared to the baseline.

TABLE I: Performance of the proposed controllers

	Nominal	IP-based design	CP-based design
$\sigma(\dot{x}_{\rm fa})$	1.00	0.55	0.58
$\sigma(\dot{\theta})$	1.00	1.05	1.06
$\sigma(\omega)$	1.00	1.00	1.02
$E_{\rm gen}$	1.00	1.00	0.98

The performances of the individual-pitch-based (IP-based) and collective-pitch-based (CP-based) controllers, normalised with respect to that of the nominal cases without any tower controller. The notation σ denotes the variance and $E_{\rm gen}$ is the energy generated.

B. Controller Performance

To showcase the use of the tower estimate, a novel individual-pitch-based tower damping control strategy is proposed that uses $\tilde{\theta}_{\rm tilt}$ as an input. The proposed strategy is compared with (i) a collective pitch-based tower controller whose input is the collective pitch $\tilde{\theta}_{\rm col}$ (e.g. [13]) and (ii) a nominal case with no tower controller. Simulations were conducted under a wind case, shown in Figure 7a, with a mean wind speed of 18 ms^{-1} and turbulence intensity of 5%. Figure 7b reveals that the tower vibrations were dampened effectively by both the proposed method and the collective pitch-based controller, with a marginal associated increase in the blade pitch activity, as shown in Figure 7c.

The key benefit of the individual-pitch-based design is that it is decoupled from the existing CPC loop, owing to the inherent properties of the Coleman transforms. This can be demonstrated by evaluating the rotor speed as shown in Figure 7d. The collective pitch-based design was coupled with the CPC due to the shared use of the collective pitch demand signals, affecting the nominal power output regulation adversely, whilst a small discrepancy can be seen between the individual-pitch-based design and nominal case, which is mainly caused by the changes in wind speed induced by the tower motion. Given that the individual-pitch-based design uses the IPC architecture, its influences on the tilt and yaw loads upon the fixed reference frame were examined in Figure 7e and 7f. Compared to the collective pitch-based design, the individual-pitch-controller imposed slightly larger tilt and yaw loads at the tower resonant frequency, upon the non-rotating turbine structure. However, relative to the peak loads, these were insignificant. Numerical results of these comparisons are summarised in Table I.

VI. Conclusion

The contributions of this paper lay in the extraction of useful additional information from existing blade load sensors and

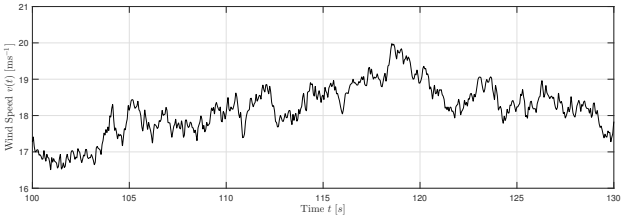

(a) Hub-height wind speed.

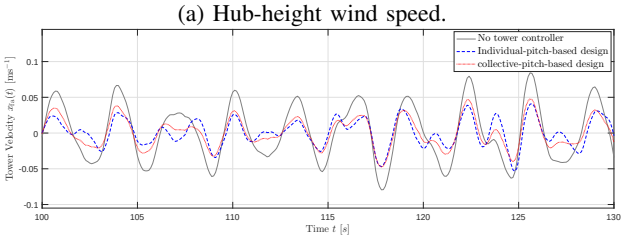

(b) Tower-top fore-aft velocity.

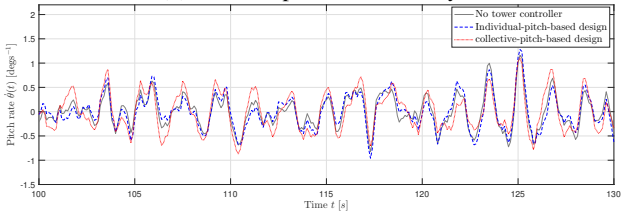

(c) Pitch rate of the blade.

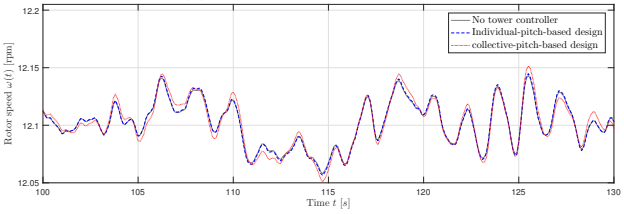

(d) Rotational speed of the rotor.

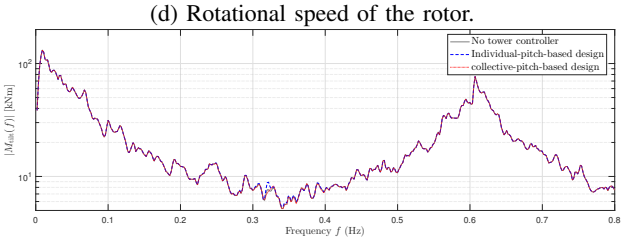

(e) Referred tilt loads on the rotor.

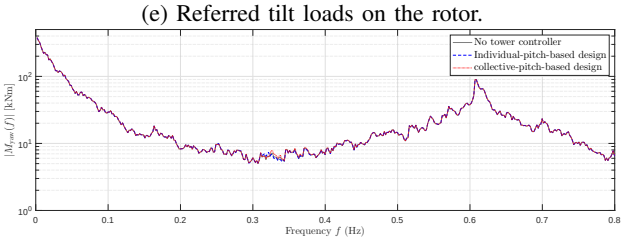

(f) Referred yaw loads on the rotor.

Fig. 7: Performance of the nominal, individual-pitch-based and collective-pitch-based controllers.

in the subsequent design of a novel individual pitch-based tower damping control strategy. The coupling between states in both rotating and fixed frames of reference led to an initial system model that was linear but time-varying, and so the Coleman Transforms were employed to manipulate this into a simpler LTI model. The key to this lay in the inclusion of the frequency splitting effects of the transforms. Having verified observability, a state estimator was synthesised that produced good estimates of the tower fore-aft motion, based solely upon the blade-load measurements. This was subsequently used in a novel individual pitch-based tower damping controller. This additional controller was augmented into a conventional controller architecture and it was shown to not interfere with the nominal power regulation loop. Closed-loop simulations upon a high-fidelity and non-linear turbine model showed good state estimates were achieved by the observer for a range of load cases covering the below-rated, above-rated and full operating wind conditions. Furthermore, the individual-pitch-based tower controller achieved similar performance compared to the collective-pitch-based approach and with no degradation on the turbine power output.

Appendix A
Proof of Theorem 3.1

Consider the azimuth angle $\phi(t) = \omega_0 t$ under one operating wind condition, the proof uses the following properties:

$$\begin{aligned}\mathcal{L}[u(t)\sin\phi(t)] &= \mathcal{L}\Big[u(t)\frac{j(e^{-j\omega_0 t} - e^{j\omega_0 t})}{2}\Big],\\ &= \frac{j}{2}\big(u(s+j\omega_0) - u(s-j\omega_0)\big), \qquad (15a)\\ \mathcal{L}[u(t)\cos\phi(t)] &= \mathcal{L}\left[u(t)\frac{e^{j\omega_0 t} + e^{-j\omega_0 t}}{2}\right],\\ &= \frac{1}{2}\big(u(s-j\omega_0) + u(s+j\omega_0)\big), \qquad (15b)\end{aligned}$$

where $u(t)$ is an arbitrary input signal and $u(s)$ is its Laplace transform. Substituting identities (15) into Coleman transformations (4) yields:

$$\begin{aligned}\begin{bmatrix}\tilde{M}_{\text{col}}(s)\\ \tilde{M}_{\text{tilt}}(s)\\ \tilde{M}_{\text{yaw}}(s)\end{bmatrix} &= \frac{2}{3}C_- \begin{bmatrix}\tilde{M}_1(s-j\omega_0)\\ \tilde{M}_2(s-j\omega_0)\\ \tilde{M}_3(s-j\omega_0)\end{bmatrix} + \frac{2}{3}C_+ \begin{bmatrix}\tilde{M}_1(s+j\omega_0)\\ \tilde{M}_2(s+j\omega_0)\\ \tilde{M}_3(s+j\omega_0)\end{bmatrix}\\ &\quad + \frac{1}{3}C_0 \begin{bmatrix}\tilde{M}_1(s)\\ \tilde{M}_2(s)\\ \tilde{M}_3(s)\end{bmatrix}, \qquad (16a)\\ \begin{bmatrix}\tilde{\theta}_1(s)\\ \tilde{\theta}_2(s)\\ \tilde{\theta}_3(s)\end{bmatrix} &= C_-^T \begin{bmatrix}\tilde{\theta}_{\text{col}}(s-j\omega_0)\\ \tilde{\theta}_{\text{tilt}}(s-j\omega_0)\\ \tilde{\theta}_{\text{yaw}}(s-j\omega_0)\end{bmatrix} + C_+^T \begin{bmatrix}\tilde{\theta}_{\text{col}}(s+j\omega_0)\\ \tilde{\theta}_{\text{tilt}}(s+j\omega_0)\\ \tilde{\theta}_{\text{yaw}}(s+j\omega_0)\end{bmatrix}\\ &\quad + C_0^T \begin{bmatrix}\tilde{\theta}_{\text{col}}(s)\\ \tilde{\theta}_{\text{tilt}}(s)\\ \tilde{\theta}_{\text{yaw}}(s)\end{bmatrix}, \qquad (16b)\end{aligned}$$

where C_-, C_+ and C_0 are defined as:

$$C_- := \frac{1}{2}\begin{bmatrix}0 & 0 & 0\\ 0 & 1 & -j\\ 0 & j & 1\end{bmatrix}\begin{bmatrix}0 & 0 & 0\\ \sin(0) & \sin(\frac{2\pi}{3}) & \sin(\frac{4\pi}{3})\\ \cos(0) & \cos(\frac{2\pi}{3}) & \cos(\frac{4\pi}{3})\end{bmatrix}, \quad (16c)$$

$$C_+ := \frac{1}{2}\begin{bmatrix}0 & 0 & 0\\ 0 & 1 & j\\ 0 & -j & 1\end{bmatrix}\begin{bmatrix}0 & 0 & 0\\ \sin(0) & \sin(\frac{2\pi}{3}) & \sin(\frac{4\pi}{3})\\ \cos(0) & \cos(\frac{2\pi}{3}) & \cos(\frac{4\pi}{3})\end{bmatrix}, \quad (16d)$$

$$C_0 := \begin{bmatrix}1 & 1 & 1\\ 0 & 0 & 0\\ 0 & 0 & 0\end{bmatrix}. \quad (16e)$$

Substituting (2) into (1a), the Laplace transform of the blade moment model (1a) becomes:

$$\begin{aligned}\tilde{M}_i(s) &= G_{M\theta}(s)\tilde{\theta}_i(s) + G_{Mv}(s)\tilde{v}_{\infty_i}(s) + G_{Mx}(s)\hat{X}_{\rm fa}(s)\\ &+ G_{M\varphi}(s)\hat{X}_{\rm fa}(s+j\omega_0) + G_{M\varphi}(s)\hat{X}_{\rm fa}(s-j\omega_0),\end{aligned} \quad (17)$$

where $\hat{X}_{\rm fa} \in \mathcal{R}$ denote the Laplace transform of $\hat{x}_{\rm fa}$. Substituting (16) into (17) yields the following Coleman-transformed model in a fixed reference frame:

$$\begin{aligned}\begin{bmatrix}\tilde{M}_{\rm col}(s)\\ \tilde{M}_{\rm tilt}(s)\\ \tilde{M}_{\rm yaw}(s)\end{bmatrix} &= \begin{bmatrix}G_{M\theta}(s) & 0 & 0\\ 0 & G^+_{M\theta}(s) & G^-_{M\theta}(s)\\ 0 & -G^-_{M\theta}(s) & G^+_{M\theta}(s)\end{bmatrix}\begin{bmatrix}\tilde{\theta}_{\rm col}(s)\\ \tilde{\theta}_{\rm tilt}(s)\\ \tilde{\theta}_{\rm yaw}(s)\end{bmatrix}\\ &+ \begin{bmatrix}G_{Mv}(s) & 0 & 0\\ 0 & G^+_{Mv}(s) & G^-_{Mv}(s)\\ 0 & -G^-_{Mv}(s) & G^+_{Mv}(s)\end{bmatrix}\begin{bmatrix}\tilde{v}_{\infty,\rm col}(s)\\ \tilde{v}_{\infty,\rm tilt}(s)\\ \tilde{v}_{\infty,\rm yaw}(s)\end{bmatrix}\\ &+ \begin{bmatrix}G_{Mx}(s)\\ G^+_{M\varphi}(s)\\ -G^-_{M\varphi}(s)\end{bmatrix}\hat{X}_{\rm fa}(s),\end{aligned} \quad (18a)$$

where the subscript $G^+, G^- \in \mathcal{R}$ are defined as:

$$G^+(s) := \frac{G(s+j\omega_0) + G(s-j\omega_0)}{2}, \quad (18b)$$

$$G^-(s) := j\frac{G(s+j\omega_0) - G(s-j\omega_0)}{2}. \quad (18c)$$

The state-space representation of (18) can be described as follows:

$$\begin{aligned}\dot{x}_{\rm b}(t) &= A_{\rm b}x_{\rm b}(t) + B_{\rm b}u_{\rm cm}(t) + B_{\rm bv}d_{\rm cm}(t) + B_{\rm bt}\dot{\tilde{x}}_{\rm fa}(t),\\ y_{\rm cm}(t) &= C_{\rm b}x_{\rm b}(t).\end{aligned} \quad (19)$$

where $A_{\rm b} \in \mathbb{R}^{n_{\rm b}\times n_{\rm b}}, B_{\rm b} \in \mathbb{R}^{n_{\rm b}\times n_{\rm u}}, B_{\rm bv} \in \mathbb{R}^{n_{\rm b}\times n_{\rm d}}, B_{\rm bt} \in \mathbb{R}^{n_{\rm b}\times n_{\rm t}}, C_{\rm b} \in \mathbb{R}^{n_{\rm y}\times n_{\rm b}}$ are time-invariant matrices (see [23]).

Next, consider the tower dynamics in (1b) which is already upon a non-rotating reference frame, and its state-space representation as follows:

$$\dot{x}_{\rm t}(t) = A_{\rm t}x_{\rm t}(t) + B_{\rm t}u_{\rm cm}(t) + B_{\rm tv}d_{\rm cm}(t),\ \dot{\tilde{x}}_{\rm fa}(t) = C_{\rm t}x_{\rm t}(t), \quad (20)$$

where $x_{\rm t}(t) = [\dot{\tilde{x}}_{\rm fa}, \tilde{x}_{\rm fa}]^T$ denotes the state of the tower dynamics.

Finally, combining (19) and (20) yields the LTI model (5), defined as follows:

$$\begin{aligned}\dot{\xi}(t) &= A_\xi\xi(t) + B_\xi u_{\rm cm}(t) + B_{\xi\rm d}d_{\rm cm}(t),\\ y_{\rm cm}(t) &= C_\xi\xi(t),\end{aligned} \quad (21a)$$

where $\xi(t) = [x_{\rm b}(t), x_{\rm t}(t)]^T \in \mathbb{R}^{n_\xi}$ and the time-invariant matrices are defined as follows:

$$A_\xi = \begin{bmatrix}A_{\rm b} & B_{\rm bt}C_{\rm t}\\ 0 & A_{\rm t}\end{bmatrix}, B_\xi = \begin{bmatrix}B_{\rm b}\\ B_{\rm t}\end{bmatrix}, B_{\xi\rm d} = \begin{bmatrix}B_{\rm bv}\\ B_{\rm tv}\end{bmatrix}, C_\xi = \begin{bmatrix}C_{\rm b} & 0\end{bmatrix}. \quad (21b)$$

REFERENCES

[1] L. Pao and K. Johnson, "A tutorial on the dynamics and control of wind turbines and wind farms," *Proc. of ACC*, 2009.

[2] E. A. Bossanyi, "Individual Blade Pitch Control for Load Reduction," *Wind Energy*, vol. 6, no. 2, pp. 119–128, 2003.

[3] K. Selvam, S. Kanev, J. W. van Wingerden, T. van Engelen, and M. Verhaegen, "Feedback-feedforward individual pitch control for wind turbine load reduction," *International Journal of Robust and Nonlinear Control*, vol. 19, no. 1, pp. 72–91, 2009.

[4] W. Leithead, V. Neilson, and S. Dominguez, "Alleviation of Unbalanced Rotor Loads by Single Blade Controllers," in *European Wind Energy Conference*, 2009.

[5] E. A. Bossanyi, "Wind Turbine Control for Load Reduction," *Wind Energy*, vol. 6, no. 3, pp. 229–244, 2003.

[6] T. J. Larsen and T. D. Hanson, "A method to avoid negative damped low frequent tower vibrations for a floating, pitch controlled wind turbine," in *Proc. of The Science of Making Torque from Wind*, 2007.

[7] P. F. Odgaard, L. F. Larsen, R. Wisniewski, and T. G. Hovgaard, "On using Pareto optimality to tune a linear model predictive controller for wind turbines," *Renewable Energy*, vol. 87, pp. 884–891, 2016.

[8] M. A. Evans, M. Cannon, and B. Kouvaritakis, "Robust MPC tower damping for variable speed wind turbines," *IEEE Transactions on Control Systems Technology*, vol. 23, no. 1, pp. 290–296, 2015.

[9] T. G. van Engelen, "Design model and load reduction assessment for multi-rotational mode individual pitch control (higher harmonics control)," in *Proc. of European Wind Energy Conference*, 2006.

[10] Q. Lu, R. Bowyer, and B. Jones, "Analysis and design of Coleman transform-based individual pitch controllers for wind-turbine load reduction," *Wind Energy*, vol. 18, no. 8, pp. 1451–1468, 2015.

[11] W. H. Lio, B. L. Jones, and J. A. Rossiter, "Preview predictive control layer design based upon known wind turbine blade-pitch controllers," *Wind Energy*, 2017.

[12] W. Leithead, V. Neilson, S. Dominguez, and A. Dutka, "A novel approach to structural load control using intelligent actuators," in *2009 17th Mediterranean Conference on Control and Automation*, pp. 1257–1262, IEEE, 2009.

[13] T. Burton, N. Jenkins, D. Sharpe, and E. Bossanyi, *Wind Energy Handbook*. Chichester, UK: John Wiley & Sons, Ltd, 2011.

[14] M. Sami and R. J. Patton, *Global wind turbine FTC via T-S fuzzy modelling and control*, vol. 45. IFAC, 2012.

[15] P. F. Odgaard and J. Stoustrup, "Fault tolerant control of wind turbines: a benchmark model," *IEEE Transactions on Control Systems Technology*, vol. 21, no. 4, pp. 1168–1182, 2013.

[16] X. Feng, R. Patton, and Z. Wang, "Sensor fault tolerant control of a wind turbine via Takagi-Sugeno fuzzy observer and model predictive control," in *2014 UKACC International Conference on Control (CONTROL)*, pp. 480–485, IEEE, 2014.

[17] P. Montagnier, R. J. Spiteri, and J. Angeles, "The control of linear time-periodic systems using FloquetLyapunov theory," *International Journal of Control*, 2004.

[18] J. Jonkman, S. Butterfield, W. Musial, and G. Scott, "Definition of a 5-MW Reference Wind Turbine for Offshore System Development," tech. rep., National Renewable Energy Laboratory (NREL), Golden, CO, 2009.

[19] W. H. Lio, J. A. Rossiter, and B. L. Jones, "Predictive control design on an embedded robust output-feedback compensator for wind turbine blade-pitch preview control," in *2016 European Control Conference*, 2016.

[20] W. H. Lio, B. L. Jones, Q. Lu, and J. A. Rossiter, "Fundamental performance similarities between individual pitch control strategies for wind turbines," *International Journal of Control*, vol. 90, no. 1, pp. 37–52, 2017.

[21] J. M. Jonkman and M. Buhl Jr., "FAST User's Guide," tech. rep., National Renewable Energy Laboratory (NREL), 2005.

[22] T. Knudsen, T. Bak, and M. Soltani, "Prediction models for wind speed at turbine locations in a wind farm," *Wind Energy*, vol. 14, pp. 877–894, 2011.

[23] W. H. Lio, B. L. Jones, and J. A. Rossiter, "Analysis and design of a tower motion estimator for wind turbines," in *2016 IEEE International Conference on Renewable Energy Research and Applications*, 2016.